Ultrahigh capacity 2 × 2 MIMO RoF system at 60 GHz employing single-sideband single-carrier modulation

Chun-Ting Lin,* Chun-Hung Ho, Hou-Tzu Huang, and Yu-Hsuan Cheng

Institute of Photonic System, National Chiao Tung University, 301, Gaofa 3rd., Guiren Township, Tainan County 711, Taiwan
**Corresponding author: jinting@mail.nctu.edu.tw*

Received December 3, 2013; revised January 21, 2014; accepted January 26, 2014;
posted January 27, 2014 (Doc. ID 202441); published March 5, 2014

This article proposes and experimentally demonstrates a radio-over-fiber system employing single-sideband single-carrier (SSB-SC) modulation at 60 GHz. SSB-SC modulation has a lower peak-to-average-power ratio than orthogonal frequency division multiplex (OFDM) modulation; therefore, the SSB-SC signals provide superior nonlinear tolerance, compared to OFDM signals. Moreover, multiple-input multiple-output (MIMO) technology was used extensively to enhance spectral efficiency. A least-mean-square-based equalizer was implemented, including MIMO channel estimation, frequency response equalization, and I/Q imbalance compensation to recover the MIMO signals. Thus, using 2 × 2 MIMO technology and 64-QAM SSB-SC signals, we achieved the highest data rate of 84 Gbps with 12 bit/s/Hz spectral efficiency using the 7-GHz license-free band at 60 GHz. © 2014 Optical Society of America

OCIS codes: (060.2330) Fiber optics communications; (060.4080) Modulation; (060.5625) Radio frequency photonics.
http://dx.doi.org/10.1364/OL.39.001358

Recently, 60-GHz technology has been highlighted for high data transmission capacity using the 7-GHz license-free band from 57 to 64 GHz, making it a strong candidate for multi-Gb/s wireless networks [1–3]. However, the wireless coverage of 60-GHz signals is limited by high propagation loss and attenuation. Radio-over-fiber (RoF) technology, comprising a fiber network with low propagation loss and cost-effective base stations, has been identified as a potential solution to extend the transmission range of 60-GHz signals. Several systems based on optical frequency multiplication have been proposed for 60-GHz RoF systems [4–6]. In addition, orthogonal frequency division multiplex (OFDM) has been used to enhance spectral efficiency in single-input single-output (SISO) systems [7]. A number of techniques based on digital signal processing, such as bit loading and I/Q imbalance compensation, have been proposed for the optimization of system performance. These techniques have enabled wireless data rates of up to 40 Gbps [8]. Furthermore, multiple-input multiple-output (MIMO) technology has attracted considerable interest as a means to improve data capacity in fiber-wireless systems [9–12]. Double-sideband single-carrier (DSB-SC) modulation with 2 × 2 MIMO technology has been demonstrated in a 60-GHz RoF system, resulting in transmissions of 27.15 Gbps [13]. To enhance spectral efficiency within the limited 7-GHz bandwidth, OFDM modulation has also been proposed using a least-mean-square (LMS) based equalizer and bit-loading algorithm, ultimately achieving data rates of 76.4 Gbps [14]. However, one major drawback of OFDM signals is a high peak-to-average power ratio (PAPR), which can result in signal performance degradation.

This Letter proposes a single-sideband single-carrier (SSB-SC) modulation in a 2 × 2 MIMO RoF system at 60 GHz. The SSB-SC signals provide better spectral efficiency than DSB-SC signals and a lower PAPR than OFDM signals. We also implemented an LMS-based equalizer, including MIMO channel estimation, frequency response equalization, and I/Q imbalance compensation for the recovery of MIMO signals [14]. Using 2 × 2 MIMO technology and 64-QAM SSB-SC signals, this study achieved the highest data rate of 84 Gbps with a spectral efficiency of 12 bit/s/Hz within the 7-GHz bandwidth following 25-km fiber and 3.5-m wireless transmission.

Figure 1 presents block diagrams of the modulation and demodulation of 2 × 2 MIMO SSB-SC signals. The block diagrams are divided into three parts: SSB-SC modulation/demodulation, MIMO decoding with equalizers, and 2 × 2 MIMO RF signal transmission. The binary data streams are divided into two independent data streams (representing the two MIMO data streams), which are mapped to the quadrature-amplitude modulation (QAM) format comprising in-phase (I) and quadrature-phase (Q) signals. Unique word sequences are added between each data block as guard intervals. This study utilized an SSB-SC matched filter comprising a suitable filter and its Hilbert transform term to realize SSB-SC modulation [15,16]. Thus, half of the spectrum of the DSB-SC signal is eliminated following I/Q signal upconversion to f_{RF} with the SSB-SC matched filter, and the generated ith stream of SSB-SC signal $S_{t,i}(f)$ can be expressed in the frequency domain as follows:

$$\begin{aligned} S_{t,i}(f) = {} & [G(f-f_{\mathrm{RF}})I_i(f-f_{\mathrm{RF}}) \\ & + jG(f-f_{\mathrm{RF}})Q_i(f-f_{\mathrm{RF}})][1+j\,\mathrm{sgn}(f-f_{\mathrm{RF}})] \\ & + [G(f+f_{\mathrm{RF}})I_i(f+f_{\mathrm{RF}}) \\ & + jG(f+f_{\mathrm{RF}})Q_i(f+f_{\mathrm{RF}})][1-j\,\mathrm{sgn}(f+f_{\mathrm{RF}})], \end{aligned} \tag{1}$$

where

$$1+j\,\mathrm{sgn}(f-f_{\mathrm{RF}}) = \begin{cases} 2, & f \geq f_{\mathrm{RF}} \\ 0, & f < f_{\mathrm{RF}} \end{cases}, \tag{2}$$

$$1-j\,\mathrm{sgn}(f+f_{\mathrm{RF}}) = \begin{cases} 0, & f \geq -f_{\mathrm{RF}} \\ 2, & f < -f_{\mathrm{RF}} \end{cases}, \tag{3}$$

where $G(f)$ represents the impulse response of the root-raised cosine filter and $-j\,\mathrm{sgn}(f)$ represents the Fourier

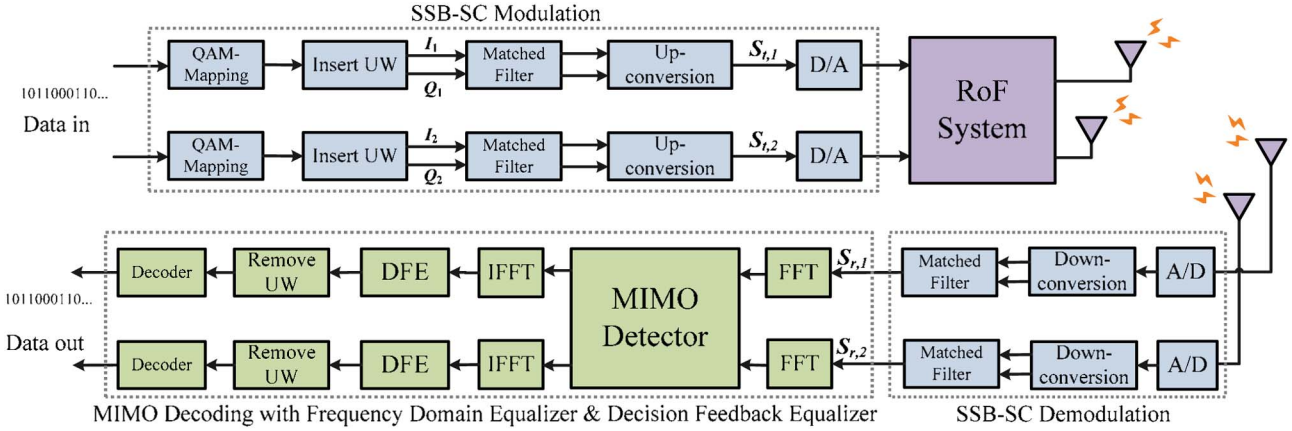

Fig. 1. Block diagrams of 2×2 MIMO SSB-SC modulation and demodulation.

transforms of the Hilbert transform, where $\mathrm{sgn}(f)$ is the sign function in the frequency domain. $I_i(f)$ and $Q_i(f)$ are frequency domain representations of in-phase and quadrature-phase signals following the Fourier transform. It should be noted that SSB signals are generated. At the receivers, the data streams after the RoF system and wireless transmission are received by two antennas. Two streams of received MIMO SSB-SC signals are down-converted and demodulated using a matched filter. Thus, the two received signals, $S_{r,1}$ and $S_{r,2}$, can be expressed as

$$\begin{bmatrix} S_{r,1}(f) \\ S_{r,2}(f) \end{bmatrix} = \begin{bmatrix} H_{11} & H_{12} \\ H_{21} & H_{22} \end{bmatrix} \begin{bmatrix} |\tilde{G}(f)|^2[I_1(f) + Q_1(f)] \\ |\tilde{G}(f)|^2[I_2(f) + Q_2(f)] \end{bmatrix} + \begin{bmatrix} W_1 \\ W_2 \end{bmatrix} = \begin{bmatrix} H_{11} & H_{12} \\ H_{21} & H_{22} \end{bmatrix} \begin{bmatrix} \Phi(f)[I_1(f) + Q_1(f)] \\ \Phi(f)[I_2(f) + Q_2(f)] \end{bmatrix} + \begin{bmatrix} W_1 \\ W_2 \end{bmatrix}, \tag{4}$$

$$\Phi(f) = |\tilde{G}(f)|^2 = |g(f)[1 + \mathrm{sgn}(f)]|^2, \tag{5}$$

where $H_{i,j}$ represents the channel coefficients in which $i = j = 1, 2$, and $\Phi(f)$ represents the transfer function of the SSB-SC matched filter in the frequency domain, which is related to the impulse response of the root-raised cosine filter. W_i denotes the additive noise. In this work, an LMS-based equalizer was utilized for channel estimation, equalization, and I/Q imbalance compensation [14]. In the block diagram presented in Fig. 2, each channel coefficient can be estimated from training symbols (TSs). The signals can be expressed as follows:

$$\begin{bmatrix} \mathrm{TS}_3 \\ \mathrm{TS}_4 \end{bmatrix} = \begin{bmatrix} H_{11} & H_{12} \\ H_{21} & H_{22} \end{bmatrix} \begin{bmatrix} \mathrm{TS}_1 \\ \mathrm{TS}_2 \end{bmatrix} + \begin{bmatrix} W_1 \\ W_2 \end{bmatrix}, \tag{6}$$

where TS_1 and TS_2 are the two transmitted TSs, and TS_3 and TS_4 are two received MIMO TSs, respectively. Hence, the transmitted data can be recovered using a zero-forcing algorithm as follows:

$$\begin{bmatrix} \bar{X}_1(f) \\ \bar{X}_2(f) \end{bmatrix} = \begin{bmatrix} \bar{H}_{11} & \bar{H}_{12} \\ \bar{H}_{21} & \bar{H}_{22} \end{bmatrix}^{-1} \begin{bmatrix} S_{r,1}(f) \\ S_{r,2}(f) \end{bmatrix} + \begin{bmatrix} \bar{H}_{11} & \bar{H}_{12} \\ \bar{H}_{21} & \bar{H}_{22} \end{bmatrix}^{-1} \begin{bmatrix} W_1 \\ W_2 \end{bmatrix}, \tag{7}$$

where $\bar{X}_1$ and $\bar{X}_2$ represent the recovered signals, and $\bar{H}_{i,j}$ denotes the estimated channel coefficients. Thus, two streams of signals can be entirely decorrelated and recovered using the zero-forcing algorithm. Each data stream is influenced by the inherent inter-symbol interference (ISI) from the Hilbert transform of the matched filter and ISI from the channel [15]. Thus, decision-feedback-equalizer (DFE) is used to compensate for these ISIs in the time domain.

Figure 3 presents the simulated complementary cumulative distribution function (CCDF) of 32-QAM SSB-SC and OFDM signals with a bandwidth of 7 GHz. The number of subcarriers of the OFDM signals is 296 with a subcarrier spacing of 23.4 MHz. For SISO signals, the PAPR values at a probability of 10^{-3} for SSB-SC and OFDM signals are 10.5 and 13.5 dB, respectively. For the 2×2 MIMO signals at the receiver side, the PAPR value at a probability of 10^{-3} for SSB-SC signals increased from 10.5 to 11.5 dB. However, the PAPR value for the OFDM signals resulted in an increase of only 0.5 dB. It should be noted that the PAPR value at a probability of 10^{-3} for

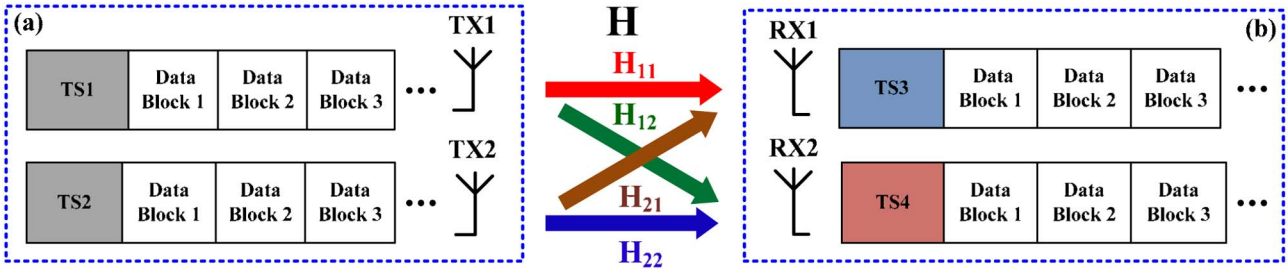

Fig. 2. Concept of 2×2 MIMO technique with unique-word sequences: (a) transmitter and (b) receiver.

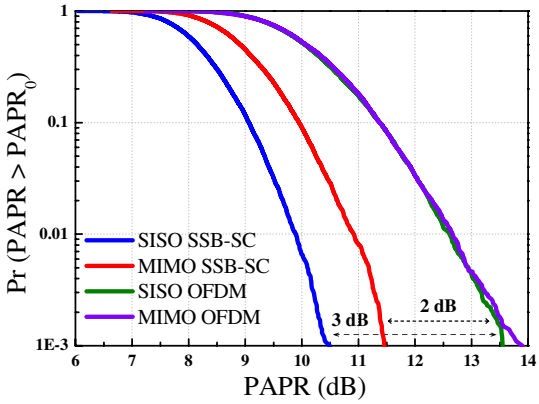

Fig. 3. CCDF diagrams of PAPR for SISO and 2 × 2 MIMO OFDM and SSB-SC signals with 32-QAM modulation format.

2 × 2 MIMO SSB-SC signals was still 2.5 dB lower than for 2 × 2 MIMO OFDM signals. Due to lower PAPR, the SSB-SC signals provided better nonlinear tolerance, compared to OFDM signals.

Figure 4 presents a schematic representation of the experimental setup of the RoF system with 2 × 2 MIMO wireless transmission at 60 GHz [8]. The optical transmitter comprised a 40-GHz single-electrode Mach–Zehnder modulator (MZM) and an electrical I/Q mixer. The I and Q channels of the SSB-SC signals were generated using an arbitrary waveform generator (AWG) with a sampling rate of 12 GHz. The I and Q signals were both sent into an electrical I/Q mixer and upconverted to 21.5 GHz. The 21.5-GHz SSB-SC signal was subsequently combined with a 39-GHz sinusoidal signal to drive the MZM. Insets (i) to (iii) in Fig. 4 describe the generation of input electrical signal into MZM. The bias voltage of the MZM was set at the null point to achieve the optical double-sideband with carrier suppression scheme. To overcome fading induced by fiber transmission, a 33/66 interleaver was implemented as an optical filter to remove undesired sidebands. The optical spectrum is presented in the inset of (a) in Fig. 5. To emulate two MIMO signals, the optical signal was spilt using a 50:50 optical coupler after fiber transmission. One of the optical signals was delayed using an additional 6-km single-mode fiber to be decorrelated with the other. After photodiode detection, the two 60.5-GHz electrical signals were generated and fed into two standard horn antennas with 23-dBi gain. Following wireless transmission over a distance of 3.5 m, the two streams of MIMO signals were received and downconverted to 5.5 GHz. The electrical spectrum of the downconverted MIMO signal is presented in inset (b) of Fig 5. These downconverted signals were captured using a scope at a sampling rate of 80 GHz and analog bandwidth of 16 GHz. The received signals were subsequently demodulated using the off-line Matlab DSP program. The bit error rate (BER) was calculated according to error count.

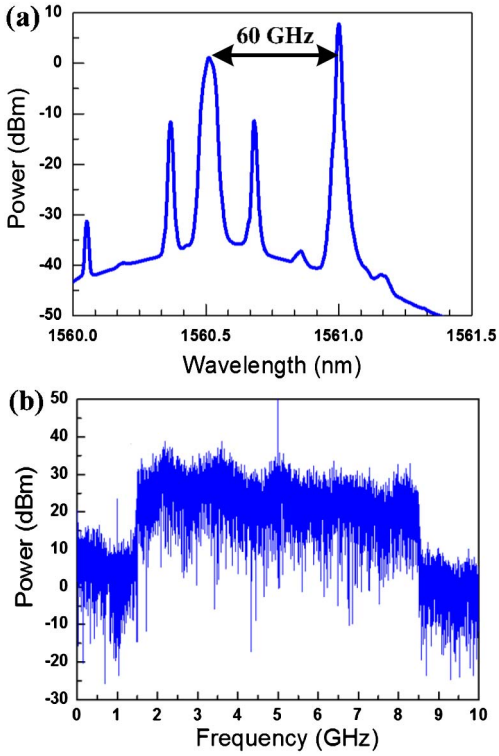

Fig. 5. Spectrum of SSB-SC signals: (a) optical and (b) electrical.

Figure 6 presents the BER curves of the 2 × 2 MIMO SSB-SC and OFDM signals. For the 32-QAM OFDM signals, the BER performance exceeded the forward error correction (FEC) threshold (1×10^{-3}) with the optical received power of −4 dBm and −3.5 dBm for the back-to-back (BTB) case and 25-km fiber transmission, respectively. The maximum data rate of the OFDM signals was 70 Gbps with a spectral efficiency of 10 bit/s/Hz. The SSB-SC signals had a lower PAPR and provided a higher signal-to-noise ratio (SNR). The 64-QAM SSB-SC signals can meet the BER below the FEC threshold in

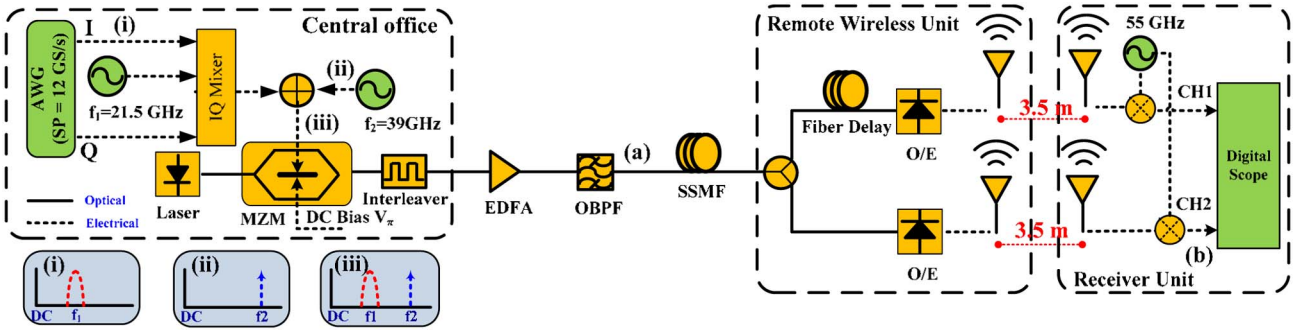

Fig. 4. Experimental setup of 2 × 2 MIMO SSB-SC RoF system at 60 GHz.

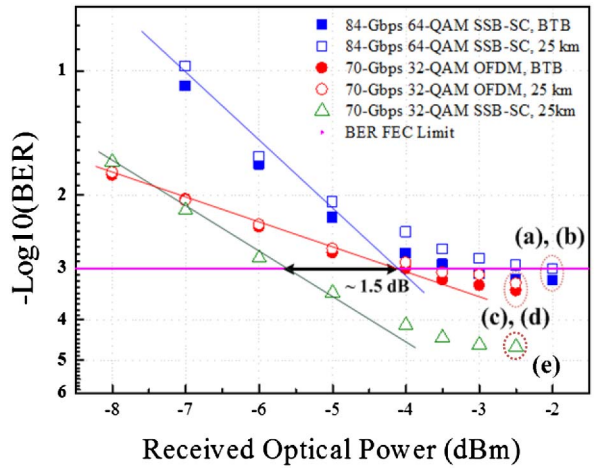

Fig. 6. BER curves comparison of 2×2 MIMO 64-QAM SSB-SC, 32-QAM OFDM signals, and 32-QAM SSB-SC signal in BTB and 25 km transmission case.

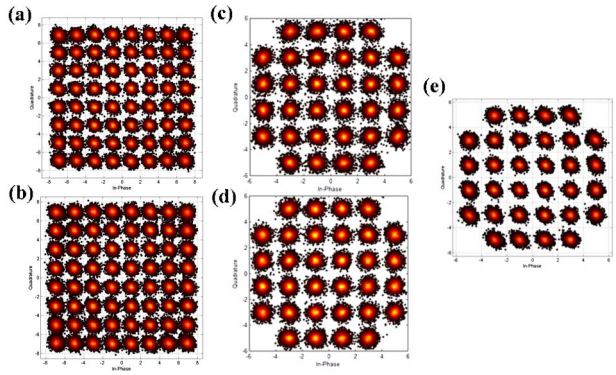

Fig. 7. Constellation diagrams of (a) BTB, 64-QAM SSB-SC signal, (b) 25-km, 64-QAM SSB-SC signal, (c) BTB, 32-QAM OFDM signal, (d) 25-km, 32-QAM OFDM signal, and (e) 25-km, 32-QAM SSB-SC signal.

the case of BTB and 25-km fiber transmission. After 25-km transmission, 32-QAM SSB-SC signals have 1.5 dB lower in received optical power than 32-QAM OFDM signals at the FEC limit. Compared with the OFDM signals, the SSB-SC signals are able to support a higher modulation format within the 7-GHz bandwidth. The SSB-SC signals attained a maximum data rate of 84 Gbps with spectral efficiency of 12 bit/s/Hz. The corresponding constellation diagrams for the SSB-SC signals and OFDM signals are presented in Figs. 7(a)–7(e). Moreover, bit-loading using a water filling algorithm can be applied to adjust the power weighting factors and re-allocate the data formats among the subcarriers of the OFDM signals. Following the application of bit-loading, the optimized data rate of the OFDM signals reached 76.4 Gbps [14]. In comparison, the data rate of SSB-SC signals is still 7.6 Gbps higher.

This Letter presents an experimental demonstration of the transmission of SSB-SC signals in a 2×2 MIMO 60-GHz RoF system. The SSB-SC signals had lower PAPR as well as the ability to support a modulation format 1 order higher than that of OFDM signals. Following 25-km fiber and 3.5-m wireless transmission, a maximum data rate of 84 Gbps with 12 bit/s/Hz spectral efficiency was achieved using 7-GHz 64-QAM SSB-SC signals.

This work was partially supported by National Science Council (NSC) of the Republic of China in Taiwan (NSC-100-2628-E-0009-019, NSC-102-2221-E-009-154).

References

1. J. Wells, IEEE Microw. Mag. **10**(3), 104 (2009).
2. R. C. Daniels and R. W. Heath, Jr., IEEE Veh. Technol. Mag. **2**(3), 41 (2007).
3. A. Stöhr, A. Akrout, R. Buß, B. Charbonnier, F. Dijk, A. Enard, S. Fedderwitz, D. Jäger, M. Huchard, F. Lecoche, J. Marti, R. Sambaraju, A. Steffan, A. Umbach, and M. Weiß, J. Opt. Commun. Netw. **8**, 471 (2009).
4. Y. T. Hsueh, Z. Jia, H. C. Chien, A. Chowdhury, J. Yu, and G. K. Chang, IEEE J. Lightwave Technol. **29**, 1105 (2011).
5. L. Zhang, M. Zhu, C. Ye, S. H. Fan, C. Liu, X. Hu, P. Cao, Q. Chang, and G. K. Chang, Opt. Express **21**, 9899 (2013).
6. C. T. Lin, J. Chen, P. T. Shih, W. J. Jiang, and S. Chi, IEEE J. Lightwave Technol. **28**, 2296 (2010).
7. M. Weiß, A. Stöhr, F. Lecoche, and B. Charbonnier, in *IEEE Proceedings of the International Topical Meeting on Microwave Photonics* (2009), pp. 1–3.
8. W. J. Jiang, H. Yang, Y. M. Yang, C. T. Lin, and A. Ng'oma, in *Proceedings of the Optical Fiber Communication Conference* (2012), paper OTu2H.1.
9. A. Ng'Oma, in *Proceedings of the Optical Fiber Communication Conference* (2012), paper OTu3E3.
10. C. Liu, A. Yi, M. Zhu, J. Wang, L. Zhang, S. C. Shih, Z. Dong, H. C. Chien, J. Yu, C. Su, G. Gu, A. Ng'oma, and G. K. Chang, in *Proceedings of the Optical Fiber Communication Conference* (2013), paper OM3D.6.
11. M. Zhu, S. H. Fan, L. Zhang, C. Liu, T. Wang, and G. K. Chang, in *Proceedings of the Optical Fiber Communication Conference* (2013), paper OTu3D.4.
12. A. Kannp, T. Kuri, I. Hosako, T. Kawanishi, Y. Yoshida, Y. Yasumura, and K. Kitayama, Opt. Express **20**, 29395 (2012).
13. C. T. Lin, A. Ng'oma, W. Y. Lee, C. C. Wei, C. Y. Wang, T. H. Lu, J. Chen, W. J. Jiang, and C. H. Ho, Opt. Express **20**, 562 (2012).
14. H. T. Huang, Y. H. Cheng, P. T. Shih, C. T. Lin, C. H. Ho, C. C. Wei, W. L. Liang, C. S. Sun, H. H. Hsu, A. Ng'oma, and S. Chi, in *Proceedings of the 39th European Conference and Exhibition on Optical Communication (ECOC)* (2013), paper Mo.3.F.2.
15. B. Pita, H. Suzuki, S. Suyama, and K. Fukawa, IEEE Trans. Veh. Technol. **57**, 311 (2008).
16. C. T. Lin, S. Y. Jian, A. Ng'oma, C. H. Ho, W. J. Jiang, C. C. Wei, and J. Chen, in *IEEE Proceedings of the International Topical Meeting on Microwave Photonics* (2011), pp. 246–249.